DOI https: //doi. org/10.1007/s11595-021-2455-1

Hypereutectic Al-Si Matrix Composites Prepared by *In Situ* Fe_2O_3/Al System

WANG Yifei[1], ZHANG Jing[1,2*], SUN Chichi[1], CHENG Zhaoxia[1], PANG Zhouyi[1], WANG Ling[3], CHEN Hongmei[4], LIU Ning[4]

(1. School of Metallurgy and Materials Engineering, Jiangsu University of Science and Technology, Zhangjiagang 215600, China; 2. Zhangjiagang Industrial Technology Research Institute, Jiangsu University of Science and Technology, Zhangjiagang 215600, China; 3. Yingkou Institute of Technology, Yingkou 115014, China; 4. School of Materials Science and Engineering, Jiangsu University of Science and Technology, Zhenjiang 212003, China)

Abstract: Al_2O_3 particles reinforced hypereutectic Al-Si composites were prepared by *in situ* Fe_2O_3/Al reaction system. The thermodynamic analysis and microstructure evolution were investigated by differential scanning calorimetry, optical microscope, scanning electronic microscopy and transmission electron microscope. Results show that the reaction between Fe_2O_3 and Al is spontaneous which can be separated into two steps at different temperatures. The *in situ* Al_2O_3 particles in nano size distribute on the Al matrix accompanied with long needle-shaped β Fe-rich intermetallic phase. With different content of Mn addition, β phase can be modified to α-$Al_{15}(Mn,Fe)_3Si_2$ and δ-$Al_4(Fe,Mn)Si_2$. Both tensile strength and elongation results at room temperature and 300 ℃ reveal that the optimal Fe-rich intermetallic phase is finer Chinese-script and polyhedral α phase with a Mn/Fe mass ratio 0.5 for the composites. Both *in situ* Al_2O_3 particles and α-Fe phases contribute to the properties improvement of the composites

Key words: hypereutectic Al-Si alloys; particles reinforced composites; Al_2O_3 particles; Fe-rich intermetallic compounds

1 Introduction

Hypereutectic Al-Si alloys are ideal materials for manufacturing engines, pistons and cylinders[1-6]. However, better mechanical properties and thermal stability are required with the increasing demands for high-performance structural materials. Particles reinforced Al-Si matrix composites have attracted a lot of attention due to their lower coefficient of thermal expansion, good wear resistance and casting properties[7-10]. Among various processing technologies of composites, the *in situ* technology is particularly attractive because of its simplicity, economy and flexibility. Oxides such as CuO, TiO_2 have been used to react with Al for synthesizing Al_2O_3/Al composites[11-14]. Usually, the *in situ* generated Al_2O_3 particles with the size around 100-200 nm have various irregular shapes and disperse uniformly in matrix. Moreover, the interface between particle and matrix is clean. The composites can be comprehensively strengthened not only by Al_2O_3 particles, but also by the high density dislocations and fine subgrains[15]. Another advantage of using metallic oxides is to introduce intermetallic compounds simultaneously with the Al_2O_3 particles which is also helpful to improve the mechanical properties.

However, there are few reports about Fe_2O_3 used to produce Al_2O_3/Al composites, especially with high Fe content. It has been studied that Fe can raise the tensile strength, creep strength and hardness of Al alloys[16,17] at high temperature. The temperature of the top of the piston can reach 250-350 ℃ when it works, so it is also valuable to consider its high-temperature strength. On the other hand, Fe is usually considered as an impurity element because of the normal long needle-like β-Al_5FeSi phase, which is detrimental to the mechanical properties due to its platelet morphology leading to a stress concentration and crack initiation[18,19]. Besides, the needle compounds tend to

(Received: Aug. 29, 2020; Accepted: July 18, 2021)

WANG Yifei(王逸飞): B D; E-mail: a1464357163@163.com

*Corresponding author: ZHANG Jing(张静): Assoc. Prof.; Ph D; E-mail: sduzhangjing@126.com

Funded by the National Natural Science Foundation of China (No.51201071), the National Natural Science Foundation of Jiangsu Province (No.BK20161270), Jiangsu Overseas Visiting Scholar Program for University Prominent Young & Middle-aged Teachers and Presidents (2018)

impede the fluidity of molten metal which is easy to lead to casting defects such as gas holes and shrinkage cavities. Mn addition is an effectively and widely studied method to replace the needle-shaped β-phase with α-Al(Mn,Fe)Si which has granular or Chinese script morphology[20-22]. Therefore, if the needle-shaped β-phase generated during the Fe_2O_3/Al *in situ* reaction system were modified by Mn, the mechanical properties could be significant improved by both the Al_2O_3 and Fe-rich phases at the same time, especially for the properties at high temperature.

Accordingly, the thermodynamic calculation of the Fe_2O_3/Al *in situ* reaction was first studied to confirm the possibility of the reaction system in present work. Then the *in situ* Al_2O_3 particles reinforced hypereutectic Al-Si composites were prepared. The effect of Mn addition on the microstructure evolution and mechanical properties was also investigated.

2 Experimental

A390 hypereutectic Al-Si alloys were used as the matrix materials in this study. The chemical composition is shown in Table 1. The *in situ* $x$$Fe_2O_3$/Al ($x$=2, 3, 9) systems were used to be the options for the reactants. Al-22 wt%Mn-7 wt%Ti master alloys were used to modify the Fe-rich intermetallic compounds generating in the *in situ* reaction.

Table 1 Chemical composition of Al-Si matrix alloys/wt%

Si	Cu	Mg	Ti	Mn	Fe	Al
17.5	4.51	0.62	0.2	0.08	0.21	Bal.

Differential scanning calorimetry (DSC) study and thermodynamic calculation were first done to confirm the feasibility of the alloy design and to select the optimal Fe_2O_3/Al system. DSC study was operated by Netzsch STA 449C differential scannig calorimetry (Netzsch, Selb, Germany). The heating rate was 10 ℃/min.

After the optimal Fe_2O_3/Al was settled, the A390 matrix alloys were first melted using an electrical resistance furnace in a graphite crucible. Fully mixed Fe_2O_3 and Al powders were introduced as the *in situ* reaction system to the molten alloys at around 850 ℃. Powder reaction system was used in present study because of more contact surfaces of Fe_2O_3 and Al powders, which is much easier to trigger the *in situ* reaction. The designed composition of the composites was A390-2Fe (2 wt% Fe coming from the *in situ* reaction between Fe_2O_3 and Al), which was studied as a prospective Al-Si-Fe alloy used for piston application[23-25]. After stirring and holding for 15 min, the Al-Mn-Ti master alloy was added into the composites. Different Mn/Fe mass ratios (0.2, 0.3, 0.5, 0.7, 0.9, 1.1) were designed to study the effect of Mn on the morphology of Fe-rich phases. The melt was poured into a steel mold after another holding for 15 min. The casting was cylindrical with a diameter of 12 mm.

Axio scope optical microscope (OM) and JSM-6480 scanning electron microscope (SEM) fitted energy dispersive X-ray spectrometer (EDS) analysis system operating at 20 kV were used to observe the morphologies of Fe-rich intermetallic phases in the composites. Specimens for OM and SEM were mechanically polished according to conventional method and were etched with Keller' s reagent. The transmission electron microscope (TEM) and high resolution transmission electron microscope (HRTEM) study of the Al_2O_3 particles were performed in a JEM-2100F electron microscopy under an accelerated voltage of 200 kV. Sample for TEM was prepared by standard methods involving mechanical grinding, polishing and dimpling followed by ion milling. The tensile strength at room temperature was tested on the Model 5582 universal tester with an extension rate of 1.0 mm/min. The specimens were plate shapes with 44 mm gauge × 12.5 mm gauge × 3 mm gauge (length × width × thickness). The tensile strength at 300 ℃ was operated on the Model5582 at a strain rate of 1.0 mm/min after holding for 30 min at 300 ℃. The specimens were rod shapes with 5 mm gauge × 30 mm gauge (diameter ×length). Ultimate tensile strength (UTS) values obtained from the engineering stress-strain curves were used to show the effect of Mn/Fe ratio on strength, because yield strength (YS) was almost the same as UTS for brittle Al-17Si-2Fe alloys[24, 25]. Elongation values were measured as the distance between the gage marks on the specimen before and after the test [26]. The elastic deformation recovered after fracture was not included.

3 Results and discussion

3.1 Thermodynamic analysis of Fe_2O_3/Al *in-situ* system

Fig.1 shows the DSC analysis results of three *in situ* Fe_2O_3/Al systems. Endothermic and exothermic peaks are found in the $2Fe_2O_3$/Al and $3Fe_2O_3$/Al, respectively. However, only one endothermic peak can be obviously detected in $9Fe_2O_3$/Al system. The endothermic peak appears at a temperature of about 660 ℃,

which is the melting point of Al. In other words, the ratio of $9Fe_2O_3$/Al system is not active to trigger the *in situ* reaction. There are two exothermic peaks in the $2Fe_2O_3$/Al and $3Fe_2O_3$/Al DSC profiles which reveals the reaction between Fe_2O_3 and Al should take place into two steps. The first exothermic peak is located around 610 ℃. Such an exothermic peak obviously corresponds to the chemical reaction between Fe_2O_3 and Al to form FeO and Al_2O_3. The possible reaction is given by the following equation:

$$2Al+3Fe_2O_3=6FeO+Al_2O_3 \quad (1)$$

The second exothermic peak is at 890 ℃ for $2Fe_2O_3$/Al and 920 ℃ for $3Fe_2O_3$/Al, which corresponds to the second reaction as shown in the following equation:

$$2Al+3FeO=3Fe+Al_2O_3 \quad (2)$$

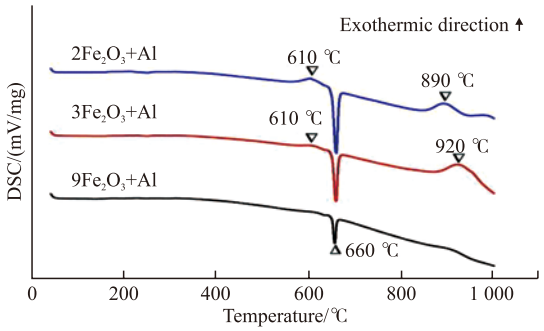

Fig.1 DSC analysis of *in-situ* reaction with different Al contents

The relationship between the Gibbs free energy and temperature of the *in situ* reaction in $2Fe_2O_3$/Al and $3Fe_2O_3$/Al is calculated by the following four equations:

$$\Delta G=x\Delta G_1+y\Delta G_2-z\Delta G_3-n\Delta G_4 \quad (3)$$

$$\Delta G=H-TS \quad (4)$$

$$H=H_{298}+\int_{298}^{T} C_{p,m}dT \quad (5)$$

$$C_{p,m}=A1+A2*10^3T+A3*10^5T^{-2}A4*10^{-6}T^2 \quad (6)$$

where ΔG is the total Gibbs free energy during reaction, ΔG_1 and ΔG_2 are the Gibbs free energy of the reaction products, ΔG_3 and ΔG_4 are the Gibbs free energy of the reactants, x, y, z, n are the chemical coefficients of reaction products and reactants in Eq.(3); H is the standard molar enthalpy, T is the temperature, S is the standard molar entropy in Eq.(4); H_{298} is the standard molar enthalpy at 298 K, $C_{p,m}$is the molar constant pressure heat capacity in Eq.(5); A1, A2, A3, A4 are the constants.

According to the DSC data, the relationship between the Gibbs free energy and temperature of $2Fe_2O_3$/Al and $3Fe_2O_3$/Al system can be concluded as:

$2Fe_2O_3$+Al system

610℃ $\Delta G=-0.69\times10^{-5}T^3+69\ 887T^2-5.02\times10^7T+8.2\times10^5T^{-1}-67.682T\ln T+1.09\times10^9$

890℃ $\Delta G=-492\ 882T^2+8.95\times10^8T-4.35\times10^8T+1\ 781.158T\ln T-4.243\times10^{11}$

$3Fe_2O_3$/Al system

610℃ $\Delta G=-0.69\times10^{-5}T^3+69\ 887T^2-5.02\times10^7T+8.2\times10^5T^{-1}-67.682T\ln T+1.09\times10^9$

920℃ $\Delta G=-4\ 207.5T^2-3.21\times10^8T+1.92\times10^6T+23.389T\ln T-2.62\times10^{12}$

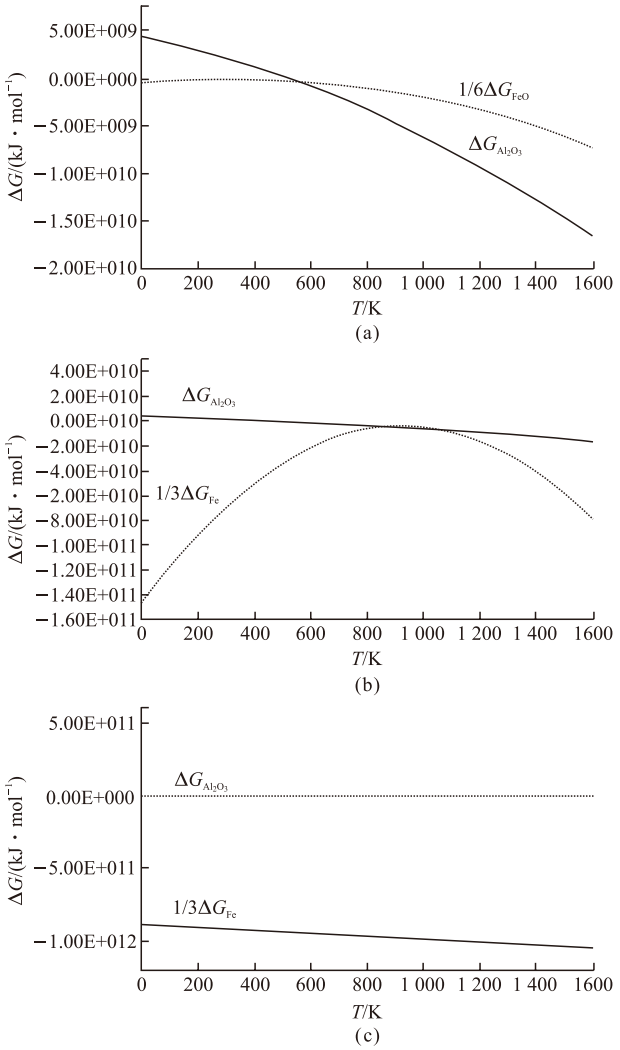

Fig.2 The curves of relationship between Gibbs free energy and temperature at different temperatures: (a)610 ℃; (b)890 ℃; (c)920 ℃

The above calculation results are drawn into Fig.2. The Gibbs free energy of Al_2O_3 is far lower than that of FeO after the temperature is higher than 883 K

(Fig.2(a)). In other words, Al_2O_3 is more stable in the Fe_2O_3/Al system in high temperature, which means it is possible to obtain composites using Fe_2O_3+Al *in situ* reaction system from the theoretical aspect. Fig.2(b) and Fig.2(c) are the relationship between Gibbs free energy and temperature in $2Fe_2O_3$/Al and $3Fe_2O_3$/Al when FeO is reduced to Fe, respectively. It can be known that the Gibbs free energy of Fe is much lower than Al_2O_3. Namely, the Fe is the more stable phase in the *in situ* reaction. Additionally, the profile of ΔG_{Fe} in$3Fe_2O_3$/Al system is almost linear compared with that of $2Fe_2O_3$/Al system which means the $3Fe_2O_3$/Al system is the better option to prepare the *in situ* composites.

3.2 Microstructure of the composite using $3Fe_2O_3$/Al *in-situ* system

According to the DSC and thermal calculation results, $3Fe_2O_3$/Al *in-situ* system was introduced to prepare the composites. The corresponding microstructure is shown in Fig.3. Fig.3(a) is the OM microstructure of the A390 matrix. Bulk primary Si and short needle-shaped eutectic Si distribute on the Al matrix. Certain amount of long needle-shaped intermetallic compound can be observed in the microstructure in A390-2Fe composite (arrows positions in Fig.3(b)). Combined with SEM image (Fig.3(c)) and the EDS results (Fig.3(d)), the compounds can be identified as Fe-rich compounds which corresponds to the β-Al_5SiFe phase.

Fig.4 is the TEM results of the *in situ* particles in the aluminum matrix. As shown in Fig.4(a) and 4(b), small black *in situ* particles (marked in circles) distribute in the matrix with the morphology of nearly ball-shape. And the sizes are in the range of several nano to dozens of nano. Besides, a large amount of high density dislocations (marked as arrows) are formed around the particles. In the other words, more volume fraction of dislocations multiply due to the nano particles in aluminum matrix. A second pattern can be observed besides the Al matrix patterns as shown in Fig.4(c), which is corresponding to the γ-Al_2O_3 . The above microstructure results (Fig.3 and Fig.4) reveal that it is possible to prepare *in situ* Al_2O_3 reinforced hypereutectic Al-Si alloys using Fe_2O_3/Al system.

It is known that the long needle-shaped β phase is detrimental to the mechanical properties. It can split the matrix under tension which provides for the racks generation and multiplication. Besides, the needle compounds tend to impede the fluidity of molten metals which is easy to lead to casting defects such as gas holes and shrinkage cavities. Two types of shrinkage pores were analyzed in the studied alloy, one small with regular shape and the other one large and elongated with dendritic arms[18,19]. Therefore, the Fe-rich intermetallic compounds of composites which generated

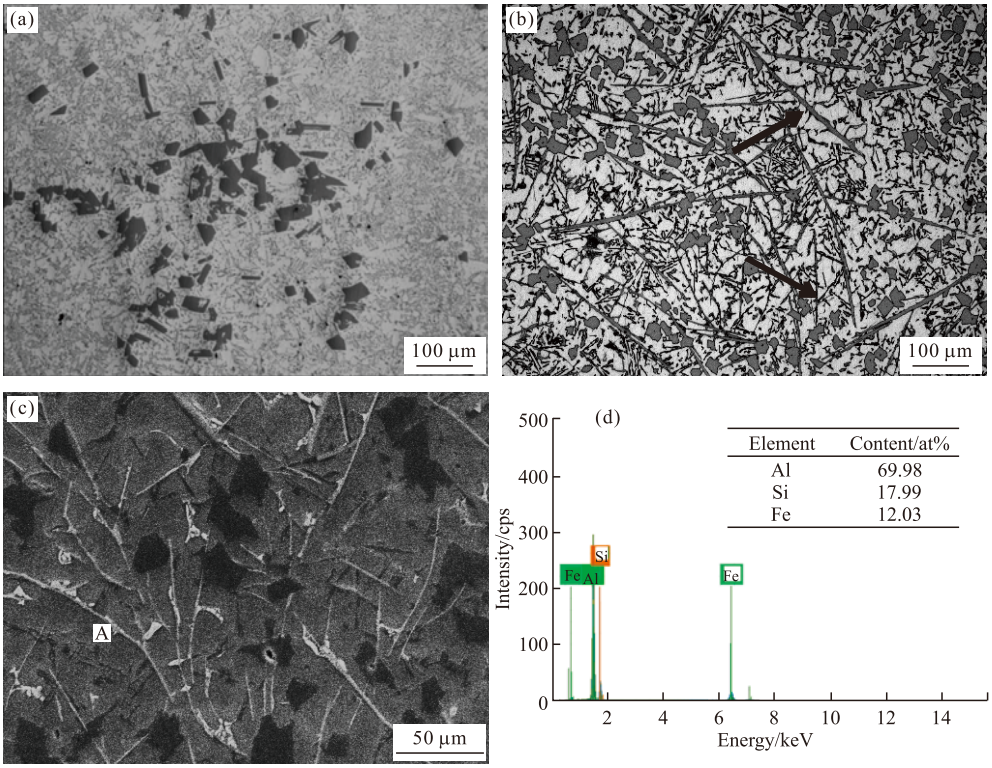

Fig.3 Comparison of microstructure in A390 with *in situ* system: (a) A390 matrix alloy; (b) OM of the composite; (c)The SEM of the composite; (d)The EDS of point A in (c)

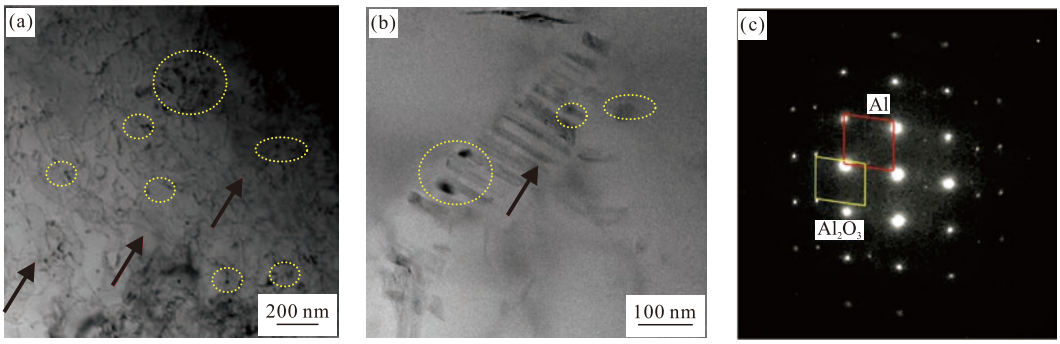

Fig.4 TEM results of the *in situ* Al_2O_3 particles in A390-2Fe composite: (a) and (b)TEM image; (c) Selected area electron diffraction patterns in (a)

during the *in situ* reaction should be modified to avoid the harmful effect on mechanical properties. Since Mn is the most effective and widely studied elements to replace the needle-shaped β-phase with less detrimental α-phase, Mn was introduced after *in situ* $3Fe_2O_3$/Al system addition. The effect of Mn/Fe mass ratios on the morphology of Fe-rich intermetallic compounds was studied.

3.3 Morphological evolution of Fe-rich phase in composites with different Mn/Fe ratios

Fig.5 is the microstructure of A390-2Fe composites with different Mn/Fe mass ratios. The schematics of various Fe-rich compounds are given in every image to show obvious evolution of the morphology. The Fe-rich phase presents as long needle-shaped without Mn addition (Fig.5(a)). Then the morphology changes to coarse plate-shaped Fe-rich intermetallic phases with Mn/Fe=0.2 (Fig.5(b)). Increasing Mn/Fe to 0.3 (Fig.5(c)), the plate-shaped Fe-rich phases keep growing until secondary arms generate, some of which separate into smaller Chinese-script and polyhedral compounds when Mn/Fe increases to 0.4 (Fig.5(d)). The intermetallic compounds mainly consist of finer Chinese-script and polyhedral compounds with the Mn/Fe=0.5 (Fig.5(e)). Then increasing the Mn/Fe to 0.7 (Fig.5(f)), 0.9 (Fig.5(g)) and 1.1(Fig.5(h)), the morphology of Fe-rich phases change inversely to dendrite, plate and coarser plate shapes, respectively.

Table 2 Elemental analysis results of the points in Fig.6/at%

Position	Al	Si	Mn	Fe
A	71.86	11.35	6.30	10.49
B	52.85	32.04	2.02	13.10

EDS analysis were operated to reveal the composition of the two typical different Fe-rich intermetallic compounds as shown in Fig.6 and Table 2. The Chinese-script and polyhedral phases consist of Al, Si, Fe and Mn four elements, which correspond to α-$Al_{15}(Mn,Fe)_3Si_2$ compounds[18,27,28]. While the composition of plate-shaped phases is close to δ- $Al_4(Fe,Mn)Si_2$ compounds[18,27,28].

According to the above microstructure results, the evolutive tendency of Fe-rich intermetallic compounds with increasing Mn/Fe from 0 to 1.1 can be described as follows: long needle-shaped β phase→ long plate-shaped ternary δ phase→ Chinese-script and polyhedral α phases → finer plate-shaped quaternary δ phase→ long plate-shaped ternary δ phase.

With lower Mn/Fe (0.2 and 0.3), Mn can replace part of Fe atoms to form quaternary intermetallic compounds which makes the aspect ratio of β phase smaller. Increasing Mn/Fe (0.4 to 0.7), the α-Fe phase is supposed to be the thermodynamic stable phase according to the phase diagram of Al-Si-Fe-Mn[26]. When Mn/Fe reaches over 0.9, δ phases prevail in the microstructure. In Becker's study[27], higher cooling rate can result in solidification path changing from α phase to $\alpha + \delta$ and δ phase in the same composition. In present work, the influence of Ti in the master alloy cannot be ignored because of higher supercooling resulting from Ti. Therefore, high Mn/Fe leads to the transformation of α to δ Fe-rich intermetallic phase.

3.4 Mechanical properties of composites

The temperature of the top of the piston can reach 250-350 ℃ when it works, so it is also valuable to consider its high-temperature strength. Tabel 3 consists the mechanical properties of as-cast A390 alloys at room temperature and at 300 ℃. Fig.7 shows the mechanical properties of the composites with different Mn/Fe mass ratios. Three Mn/Fe ratios (0.3, 0.5 and 0.9) with three typical Fe-rich intermetallic phases were chosen to show the mechanical evolution. Without Mn addi-

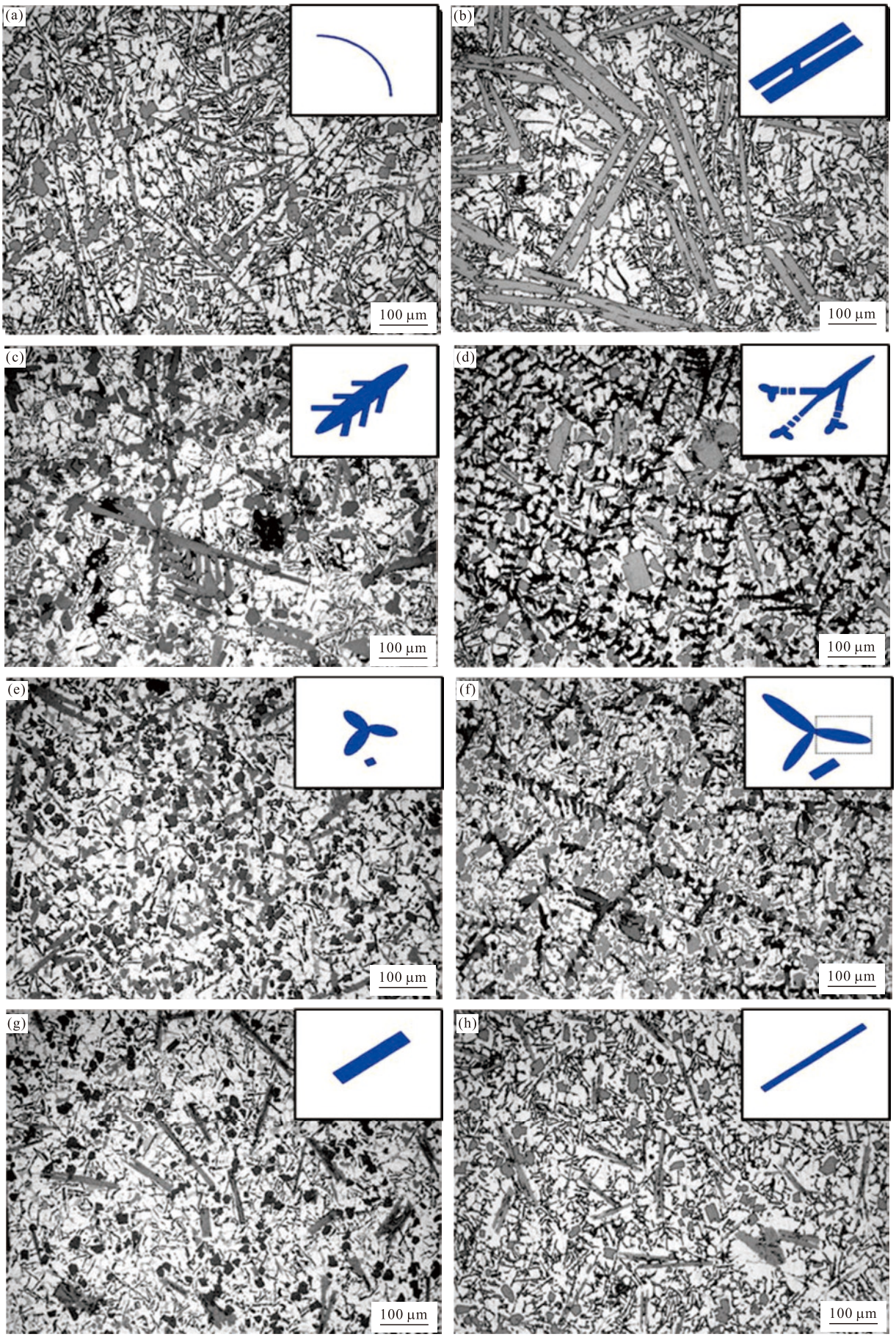

Fig.5 Microstructure of composites with different Mn/Fe: (a) 0; (b) 0.2; (c) 0.3; (d) 0.4; (e) 0.5; (f) 0.7; (g) 0.9; (h) 1.1

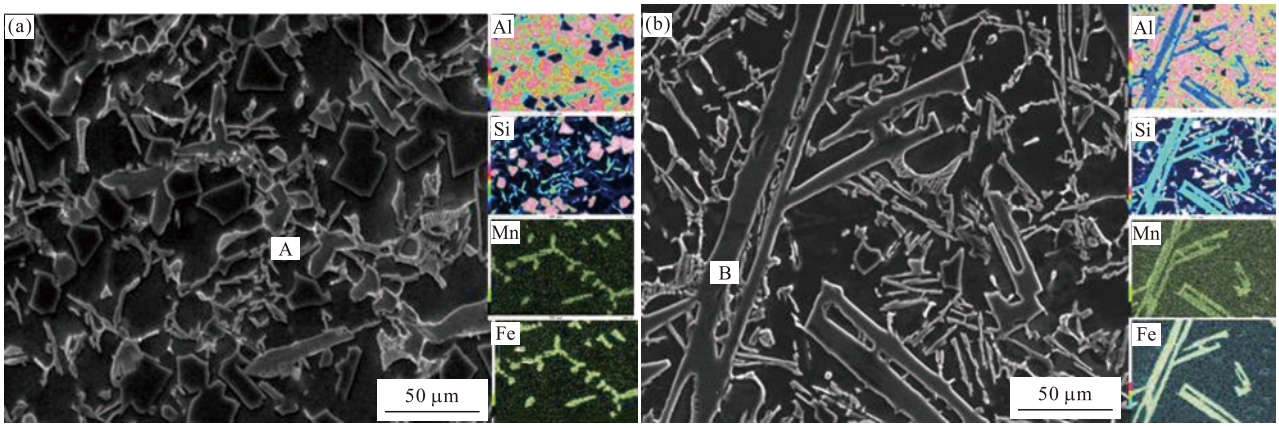

Fig.6 EDS mapping results of different Fe-rich intermetallic compounds: (a) Chinese-script and polyhedral compounds; (b) Plate-shaped compounds

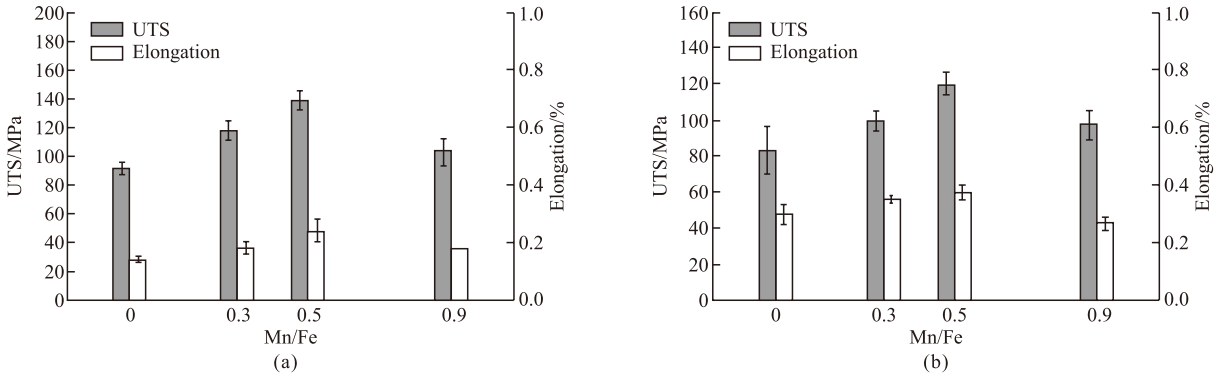

Fig.7 Tensile properties of composites with different Mn/Fe ratios: (a) Room temperature; (b) 300 ℃

tion, the ultimate tensile strengths at room temperature decrease because the long needle-shaped β phase split the matrix under tension which provides for the racks generation and multiplication. Additionally, casting defects such as gas holes and shrinkage cavities can be easily generated due to β phase. With Mn/Fe increasing from 0.3 to 0.5, the UTS improves by 29%, 52% at room temperature and 19%, 44% at 300 ℃, respectively. The modified Chinese-script and polyhedral α-Fe compounds have less negative effect on the matrix and are more stable at high temperature which results in better mechanical properties. However, the UTS of the composite with 0.9 Mn/Fe is a little lower. Plate-shaped δ Fe-rich phases have a larger length-width ratio than α-Fe compounds which is the reason for the slight decrease of UTS and elongation when Mn/Fe reaches up to 0.9. The elongation evolution has a similar tendency with the increasing of Mn/Fe ratio. And the elongation increase slightly at 300 ℃ compared with that at room temperature. That's because the grain boundaries slipping becomes much easier at high temperature which results in higher elongation value compared with the one at room temperature. Accordingly, the A390-2Fe composite with finer Chinese-script and polyhedral α-Fe compounds (Mn/Fe=0.5) has the optimal mechanical properties.

Table 3 Mechanical properties of as-cast A390 alloys

Item	UTS/MPa	Elongation/%
Room temperature	104.59	1.7
300 ℃	67.55	2.1

The *in situ* Al_2O_3 particles play another important role for the mechanical properties improvement. Al_2O_3 particles are hard second phases which cannot be cutted-trough by dislocations. Therefore, the effect can be concluded as Orowan mechanism which is shown in the following equation:

$$\sigma_{\text{orowan}}=\frac{G_m b}{\pi(1-v)^{\frac{1}{2}}}\frac{1}{D\left(\frac{\pi}{6v_f}-\frac{2}{3}\right)^{\frac{1}{2}}}\ln(D/b) \quad (7)$$

where σ_{orowan} is the stress, G_m is the shear modulus of the matrix, b is the Burgers vector, v is the Poisson's ratio, V_f is the volume fraction of particles and D is the diameter of the particles.

The stress is inversely proportional to the size of the particles. In present work, the *in situ* Al_2O_3 particles are in nano size which could provide high strengthening effect. As seen in Fig.4, dislocation loops around Al_2O_3 particles can be observed. The dislocation multiplication through Orowan mechanism also contributes to the mechanical improvement of the composites.

4 Conclusions

a) DSC and thermodynamic calculation results reveal that it is possible to prepare *in situ* Al_2O_3 reinforced hypereutectic Al-Si alloys using Fe_2O_3/Al system. Experimental results confirm the feasibility on the other hand. *In situ* Al_2O_3 particles in nano size distribute on the Al matrix accompanied with long needle-shaped β Fe-rich intermetallic phase.

b) The evolutive tendency of Fe-rich intermetallic compounds with increasing Mn/Fe mass ratio from 0 to 1.1 can be described as follows: long needle-shaped β phase→ long plate-shaped ternary δ phase → Chinese-script and polyhedral α phases → finer plate-shaped quaternary δ phase→ long plate-shaped ternary δ phase.

c) Both the tensile strength and elongation at room temperature and 300 ℃ increase first and then decrease a little with the Mn/Fe increasing. The A390-2Fe composite with finer Chinese-script and polyhedral α-Fe compounds (Mn/Fe=0.5) has the optimal mechanical properties. Chinese-script and polyhedral α-Fe compounds and *in situ* nano Al_2O_3 particles contribute to the mechanical properties improvement.

References

[1] Jiao X Y, Wang J, Liu C F, *et al.* Influence of Slow-shot Speed on PSPs and Porosity of AlSi17Cu2.5 Alloy During High Pressure Die Casting[J]. *J. Mater. Process. Tech*., 2019, 268: 63-69

[2] Yu W B, Zhao H B, Wang L, *et al.* The Influence of T6 Treatment on Fracture Behavior of Hypereutectic Al-Si HPDC Casting Alloy[J]. *J. Alloy. Compd.*, 2018, 731: 444-451

[3] Gietzelt T, Wunsch T, Messerschmidt F, *et al*. Influence of Laser Welding Speed on the Morphology and Phases Occurring in Spray-compacted Hypereutectic Al-Si Alloys[J]. *Metals*, 2016, 6(12): 295

[4] Wang J, Guo Z, Song J L, *et al*. On the Growth Mechanism of the Primary Silicon Particle in a Hypereutectic Al-20 wt%Si Alloy Using Synchrotron X-ray Tomography[J]. *Mater. Design*, 2018, 137: 176-183

[5] Jeon J H, Shin J H, Bae D H. Si Phase Modification on the Elevated Temperature Mechanical Properties of Al-Si Hypereutectic Alloys[J]. *Mater. Sci. Eng. A*, 2019, 748(6): 367-370

[6] Liu T T, Pang X X, Xian Y J, *et al.* Effect of Al_2O_{3np} on the Properties and Microstructure of B_4C_p/Al Composites[J]. *J. Wuhan University of Technology-Mater. Sci. Ed.*, 2020, 35: 514-519

[7] Chen G Q, Yang W S, Xin L, *et al.* Mechanical Properties of Al Matrix Composite Reinforced with Diamond Particles with W Coatings Prepared by the Magnetron Sputtering Method[J]. *J. Alloy. Compd*., 2018, 735: 777-786

[8] Monje I E, Louis E, Molina J M. Interfacial Nano-engineering in Al/Diamond Composites for Thermal Management by *in situ* Diamond Surface Gas Desorption[J]. *Scripta Mater*., 2016, 115: 159-163

[9] Li P T, Li Y G, Wu Y Y, *et al.* Distribution of TiB_2 Particles and Its Effect on the Mechanical Properties of A390 Alloy[J]. *Mater. Sci. Eng. A*, 2012, 546: 146-152

[10] Wu C C, Gao T, Sun Q Q, *et al*. A Novel Method of Coating *Ex-situ* SiC Particles with *In-situ* SiC Interlayer in Al-Si-C Alloy[J]. *J. Alloy. Compd*., 2018, 754: 39-47

[11] Fan T, Zhang D, Yang G, *et al.* Fabrication of *In situ* Al_2O_3/Al Composite via Remelting[J]. *J. Mater. Process. Tech*., 2013, 142(2): 556-561

[12] Maity P, Chakraborty P, Panigrahi S. Preparation of Al-$MgAl_2O_4$-MgO *In Situ* Particle-composites by Addition of MnO_2 Particles to Molten Al-2 wt% Mg Alloys[J]. *Mater. Lett*., 1994, 20 (3-4): 93-97

[13] Padmavardhani D, Gomez A, Abbaschian R. Synthesis and Microstructural Characterization of NiAl/Al_2O_3 Functionally Gradient Composites[J]. *Intermetallics*, 1998, 6(4): 229-241

[14] Yang B, Sun M, Gan G S, *et al. In Situ* Al_2O_3 Particle-reinforced Al and Cu Matrix Composites Synthesized by Displacement Reactions[J]. *J. Alloy. Compd.*, 2010, 494(1-2): 261-265

[15] Wang H M, Li G R, Zhao Y T, *et al. In Situ* Fabrication and Microstructure of Al_2O_3 Particles Reinforced Aluminum Matrix Composites[J]. *Mater. Sci. Eng. A*, 2010, 527(12): 2 881-2 885

[16] Lin C, Wu S S, Zhong G, *et al*. Effect of Ultrasonic Vibration on Fe-containing Intermetallic Compounds of Hypereutectic Al-Si Alloys with High Fe Content[J]. *T. Nonferr. Metal. Soc. China*, 2013, 23(5): 1 245-1 252

[17] Lin C, Wu S S, Lü S L, *et al.* Influence of High Pressure and Manganese Addition on Fe-rich Phases and Mechanical Properties of Hypereutectic Al-Si Alloy with Rrheo-squeeze Casting[J]. *T. Nonferr. Metal. Soc. China*, 2019, 29(2): 253-262

[18] Becker H, Bergh T, Vullum P E, *et al. β*- and *δ*-Al-Fe-Si Intermetallic Phase, Their Intergrowth and Polytype Formation[J]. *J. Alloy. Compd*., 2019, 780: 917-929

[19] Wu Y N, Liao H C. Corrosion Behavior of Extruded Near Eutectic Al-Si-Mg and 6063 Alloys[J]. *J. .Mater. Sci. Tech.*, 2013, 29(4): 380-386

[20] Gao T, Hu K Q, Wang L S, *et al*. Morphological Evolution and Strengthening Behavior of α-Al(Fe,Mn)Si in Al-6Si-2Fe-*x*Mn Alloys[J]. *Results Phys*., 2017, 7: 1 051-1 054

[21] Gao T, Wu Y Y, Li C, *et al*. Morphologies and Growth Mechanisms of α-Al(FeMn)Si in Al-Si-Fe-Mn Alloy[J]. *Mater. Lett*., 2013, 110: 191-194

[22] Öz T, Karaköse E, Keskin M. Impact of Beryllium Additions on Thermal and Mechanical Properties of Conventionally Solidified and Melt-spun Al-4.5 wt%Mn-*x* wt%Be (*x* = 0, 1, 3, 5) Alloys[J]. *Mater. Design*, 2013, 50: 399-421

[23] Todaro C J, Easton M A, Qiu D, *et al.* Effect of Ultrasonic Melt Treatment on Intermetallic Phase Formation in a Manganese-modified Al-17Si-2Fe Alloy[J]. *J. Alloy. Compd*., 2019, 271: 346-356

[24] Lin C, Wu S S, Lü S L, *et al.* Effects of Ultrasonic Vibration and Manganese on Microstructure and Mechanical Properties of Hypereutectic Al-Si Alloys with 2%Fe[J]. *Intermetallics*, 2013, 32: 176-183

[25] Lin C, Wu S S, Lü S L, *et al*. Microstructure and Mechanical Properties of Rheo-diecast Hypereutectic Al-Si Alloy with 2%Fe Assisted with Ultrasonic Vibration Process[J]. *J. Alloy. Compd*., 2013, 568: 42-48

[26] Askeland D R, Phule P P. *Essentials of Materials Science and Engineering*[M]. Columbia: Thomson, 2005

[27] Chen H L, Chen Q, Du Y, *et al.* Update of Al-Fe-Si, Al-Mn-Si and Al-Fe-Mn-Si Thermodynamic Descriptions[J]. *T. Nonferr. Metal. Soc. China*, 2014, 24(7): 2 041-2 053

[28] Becker H, Bergh T, Vullum P E, *et al.* Effect of Mn and Cooling Rates on *α*-, *β*- and *δ*-Al-Fe-Si Intermetallic Phase Formation in a Secondary Al-Si Alloy[J]. *Materialia*, 2019, 5: 100 198